Temperature influences on the performance of a dielectric elastomer generator with consideration of dissipation processes and failures

***Shoue Chen[1], †Zhicheng He[1], Eric Li[2]**

[1]State Key Laboratory of Advanced Design and Manufacturing for Vehicle Body, Hunan University, China

[2]Department of Mechanical and Automation Engineering, The Chinese University of Hong Kong, China

*Presenting author: chenshoue725@163.com

†Corresponding author: hezhicheng815@163.com

Abstract

As a category of promising material, the membrane of dielectric elastomer (DE) sandwiched between two compliant electrodes has the capacity for converting the electrical energy into mechanical energy, vice versa. Owing to the large deformation produced by relatively small stimulations, this elastomer is also component to function as a generator. Investigations on the dielectric elastomer generator (DEG) have achieved wide attention recently. The previous studies have indicated that the performance of DE depends on the major dissipation processes including viscoelasticity and current leakage and also varies with temperature. However, very few works take these factors together into consideration when investigating the performance of DEGs. Therefore, a model that involves the temperature-dependent permittivity and shear modulus of the DE membrane, viscoelastic relaxation and current leakage is established in this study. Then, based on a specific Carnot-shape conversion cycle, the performances of the dissipative generator made of very-high-bond (VHB) elastomer can be discussed at different sampling temperatures. The parameters characterizing the performances of the DEG include the energy densities of different kinds and conversion efficiency. Moreover, the mechanisms of typical failure modes including material rupture, loss of tension (LT), electrical breakdown (EB) and electromechanical instability (EMI) are studied with the influences of temperature to ensure that the generator is operated in an allowable area. It can be concluded from the numerical results that the temperature plays an important role in the performance of the DEG, which could possibly improve its conversion efficiency.

Keywords: Dielectric elastomer generators (DEGs); Temperature; Failure modes; Dissipation processes;

1. Introduction

The dielectric elastomer (DE) which appears as a thin membrane is often coated with softly conductive electrodes on both sides in thickness [1]-[4]. When subject to a voltage through its thickness, the membrane of DE will shrink in thickness and expand in area due to Maxwell stress, converting the electrical energy into mechanical energy, which can be exploited as an actuator [5]-[7]. Owing to the large deformation caused by small mechanical forces and an appropriate voltage, the DE membrane is also competent to function as a generator [8]-[10]. When a membrane of DE operates under cyclic loadings, the reduction in tensile force will lead to the enhancement in both the thickness and voltage through the electrodes, converting the mechanical energy into electrical energy. Nowadays, there is an increasing attention on the field of dielectric elastomer generator (DEG). For instance, a heel-strike generator made of DE has been implanted into shoes [11], a membrane device placed behind the knee is able

to recycle the energy from human motion [12], and even a wave power generator made of DE has been developed for harvesting renewable energy [13].

Being a generator, except the unavoidable dissipation processes including viscoelasticity and current leakage [14], the DE membrane may lose efficacy due to multiple failure modes, such as material rupture, loss of tension (LT), electrical breakdown (EB), and electromechanical instability (EMI) [15]-[22], which may restrict the area of allowable states during the energy harvesting. As a result, it is of great importance to study the mechanism of failure modes for advanced development of DEGs.

Most of the previous studies on the electromechanical performance of DE were implemented in an isothermal environment but ignored the influences of temperature [23][24]. However, according to the experiments on very-high-bond (VHB) elastomers [25][26], there is a strong dependency between the relatively permittivity and the planar stretches of the DE membrane at different operating temperatures. The shear modulus of the membrane of DE is also proved to be related with temperature and the relationship will not be described by the T/T_0 factor anymore. To the authors' best knowledge, there is few research on the effects of temperature on both electromechanical performance and energy conversion of DEGs.

In this study, the most promising DE material, VHB 4910, which has high electromechanical conversion efficiency and can produce a large deformation within a wide temperature range (233~363 K) [26] is selected to study the effect of temperature on the performance of DEGs. For the first time, an integrated model that combines the temperature-dependent permittivity and shear modulus, current leakage and viscoelasticity is established to simulate the energy harvesting. Afterwards, the mechanism and processes of a four-stroke conversion cycle for the DEG is introduced. Based on the cyclic loads, different energies as well as the conversion efficiency can be figured out. By comparing the numerical results at different temperatures, one can summarize the temperature influence on the DEG. At the same time, common failure modes of the DE membrane are taken into consideration to ensure the allowable states.

2. Governing equations for the dissipative DEG

To focus on the influences of temperature on the electromechanical performance of the DEG, the governing equations for the membrane of DE should be first derived and can be separated into the following parts: (1) the free energy function of DE with consideration of viscoelastic relaxation and temperature-related factors; (2) equations of the plane-parallel capacitor; (3) equations of the current leakage. These segments constitute the integrated equations of state for the DEG.

2.1. Free energy function of the DE membrane

A fundamental configuration is utilized to conduct the simulation, in which a thin membrane of VHB 4910 is sandwiched between two electrodes with negligible electrical resistance and mechanical stiffness. Subject to in-plane biaxial forces P_1 and P_2 and a voltage Φ in thickness, the membrane deforms from its initial dimensions $L_1\times L_2\times H$ to the current dimensions $l_1\times l_2\times h$ with charges of opposite sign $\pm Q_p$ generated on the electrodes at a fixed temperature T, as demonstrated in Fig. 1. As a homogeneous and isotropic elastomer, the stretches in plane can be defined as $\lambda_i=l_i/L_i$ (i=1,2), while the stretch in thickness direction can be substituted by $\lambda_1^{-1}\lambda_2^{-1}$ due to the nearly-incompressibility of the membrane [2][27]. Similarly, the nominal stresses in plane are defined by $s_1=P_1/(L_2H)$, $s_2=P_2/(L_1H)$. In electrical category, $\tilde{E}=\Phi/H$

and $\tilde{D}=Q_p/(L_1L_2)$ represent the nominal electric field and the nominal electric displacement, respectively.

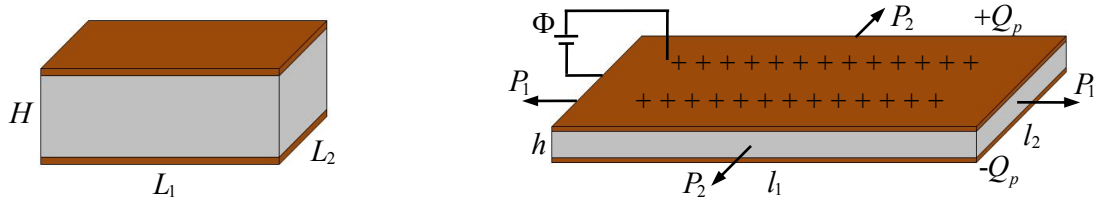

(a) (b)

Figure 1. Schematic of the DE membrane in (a) undeformed state; (b) deformed state, subject to forces and a voltage at a fixed temperature *T;*

Due to obvious viscoelasticity, the membrane of DE will no longer show the simple elasticity during the deformation. According to the recent studies [28]-[31], the viscoelastic relaxation can be simulated by a nonlinear rheological model, as illustrated in Fig. 2. The viscoelastic model consists of two parallel networks: spring *A* in parallel with spring *B* and a dashpot with a viscosity η. Factors μ^A and μ^B represent the shear moduli of the springs which vary with temperature, J^A and J^B are the dimension parameters referring to the dependence on chain extension limits of the elastomer. It is assumed that J^A and J^B are independent of temperature.

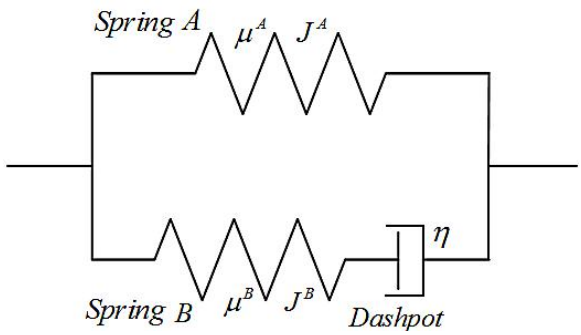

Figure 2. Viscoelasticity of the DE membrane is modeled by a rheological model.

In the rheological model, the stretch of the DE membrane in a certain direction is equal to the net stretches in both networks. For spring *A*, the stretch in it is the same as the stretch of the membrane λ. While the stretch of the spring *B* is described by λ^e, which cooperates with the inelastic stretch ξ due to the dashpot. A well-established rule [14] is chosen to represent the relationship between these stretches, $\lambda=\lambda^e\xi$.

In order to measure the mechanical work done by the dashpot, that is, the energy dissipated by the viscoelasticity during the harvesting, the condition of stress in the rheological model should also be solved. When subject to mechanical forces in plane and a voltage in thickness, the DE membrane will be stretched by λ due to the stress arising form the force σ_{force} and the Maxwell stress $\sigma_{Maxwell}$. The sum of the external stresses should be balanced by the stresses in both networks, $\sigma^A+\sigma^B=\sigma_{Maxwell}+\sigma_{force}$, where the stress in spring *A* equals the stress in the top network σ^A, and the stress acting on the dashpot is the same as the stress in spring *B*, which is also the stress in the bottom network σ^B.

Previously, the permittivity of DE is assumed as constant in the majority of cases, which goes against the molecular physics: molecules in the elastomer will contain more thermodynamic energy at a higher temperature, resulting in a greater amplitude of random thermal motion.

Therefore, the molecules are less closely aligned with each other, and the relative permittivity will decline with the enhancement in temperature. The stretch will change the active range of the molecules too [32]. Indeed, the recent research has proved that the relative permittivity of VHB 4910 is affected by the temperature and stretch simultaneously [26], and the specific expression of ε_r for VHB 4910 can be depicted in Eq. (1).

$$\varepsilon_r(\lambda_1,\lambda_2,T) = a\lambda_1\lambda_2 + \frac{b}{T} + c \tag{1}$$

where a is the parameter describing the electrostriction of DE, and b is determined by the expression $M\eta_d^2/(3\kappa\varepsilon_0)$, where M, η_d and κ represent the dipole current density, the dipole moment and the Boltzmann constant, respectively. ε_0=8.85×10^{-12} F/m is the permittivity of vacuum. Parameter c describes the relative permittivity at the reference temperature without deformation. The parameters obtained from the experimental data of Jean-Mistral [26] will be selected here: a=-0.0533 F/m, b=645.4224 F.K/m and c=3.1834 F/m.

The dielectric elastomer itself, the mechanical forces, the external voltage and the thermal force constitute a thermodynamic system, and the free energy density function of this system can be expressed as follows:

$$W = W_s(\lambda_1,\lambda_2,T) + \frac{\tilde{D}^2}{2\varepsilon_0\varepsilon_r(\lambda_1,\lambda_2,T)}\lambda_1^{-2}\lambda_2^{-2} + \rho_0 c_0\left[T - T_0 - T\ln(\frac{T}{T_0})\right] \tag{2}$$

where the thermo-elastic energy W_s denotes the variation in strain energy from the reference configuration to the current configuration at a fixed temperature T. The electrostatic energy is represented by the second item in the right hand side of Eq. (2). The last item reflects the absolute thermal contribution [18][19], in which the density and the specific heat capacity of the DE film are described by ρ_0 and c_0, respectively.

In practice, the VHB elastomer exhibits strain-stiffening effect during the deformation due to finite configurations of the polymer chains [2][32]. Considering the extension limits, the Gent model [33] is adopted to characterize the thermo-elastic energy W_s. Combine the rheological model and the relative permittivity of VHB 4910, the specific function of W_s can be described in Eq. (3).

$$\begin{aligned} W_s = &-\frac{\mu^A(T)J^A}{2}\ln\left(1-\frac{\lambda_1^{\,2}+\lambda_2^{\,2}+\lambda_1^{-2}\lambda_2^{-2}-3}{J^A}\right) - \frac{\mu^B(T)J^B}{2}\cdot \\ &\ln\left(1-\frac{\lambda_1^{\,2}\xi_1^{-2}+\lambda_2^{\,2}\xi_2^{-2}+\lambda_1^{-2}\lambda_2^{-2}\xi_1^{\,2}\xi_2^{\,2}-3}{J^B}\right) \end{aligned} \tag{3}$$

where the shear moduli of the springs meet the relation, μ^A/μ^B=3/7 [14] and an instantaneous modulus of DE is defined as $\mu(T)=\mu^A+\mu^B=Y(T)/3$, where $Y(T)$ stands for the isothermal elastic modulus in small deformation at temperature T. In this study, a set of material parameters for

VHB 4910 are chosen as: J^A=90, J^B=30 [34] and $Y(T)$=0.2001(1000/T)^2-1.078(1000/T)+1.518 MPa [35].

According to the equilibrium in thermodynamics, when the DE membrane is in mechanical and electrical equilibrium, the equations of state can be achieved from: $s_1=\partial W/\partial\lambda_1$, $s_2=\partial W/\partial\lambda_2$ and $\tilde{E}=\partial W/\partial\tilde{D}$ [2][16]. The specific equations of state are demonstrated in Eqs. (4)-(6).

$$s_1=\frac{\mu_B(T)(\lambda_1\xi_1^{-2}-\lambda_1^{-3}\xi_1^{2}\lambda_2^{-2}\xi_2^{2})}{(1-(\lambda_1^{2}\xi_1^{-2}+\lambda_2^{2}\xi_2^{-2}+\lambda_1^{-2}\lambda_2^{-2}\xi_1^{2}\xi_2^{2}-3)/J_B)}+\frac{\mu_A(T)(\lambda_1-\lambda_1^{-3}\lambda_2^{-2})}{(1-(\lambda_1^{2}+\lambda_2^{2}+\lambda_1^{-2}\lambda_2^{-2}-3)/J_A)}-\frac{\tilde{D}^2}{\varepsilon_0(a\lambda_1\lambda_2+b/T+c)\lambda_1^{3}\lambda_2^{2}}-\frac{a\tilde{D}^2}{2\varepsilon_0(a\lambda_1\lambda_2+b/T+c)^2\lambda_1^{2}\lambda_2} \tag{4}$$

$$s_2=\frac{\mu_B(T)(\lambda_2\xi_2^{-2}-\lambda_2^{-3}\xi_1^{2}\lambda_1^{-2}\xi_2^{2})}{(1-(\lambda_1^{2}\xi_1^{-2}+\lambda_2^{2}\xi_2^{-2}+\lambda_1^{-2}\lambda_2^{-2}\xi_1^{2}\xi_2^{2}-3)/J_B)}+\frac{\mu_A(T)(\lambda_2-\lambda_2^{-3}\lambda_1^{-2})}{(1-(\lambda_1^{2}+\lambda_2^{2}+\lambda_1^{-2}\lambda_2^{-2}-3)/J_A)}-\frac{\tilde{D}^2}{\varepsilon_0(a\lambda_1\lambda_2+b/T+c)\lambda_1^{2}\lambda_2^{3}}-\frac{a\tilde{D}^2}{2\varepsilon_0(a\lambda_1\lambda_2+b/T+c)^2\lambda_1\lambda_2^{2}} \tag{5}$$

$$\tilde{E}=\frac{\tilde{D}}{\varepsilon_0(a\lambda_1\lambda_2+b/T+c)\lambda_1^{2}\lambda_2^{2}} \tag{6}$$

The membrane is subject to a homogeneous, equal-biaxial force P in the following simulation, so setting $s_1=s_2=s$, $\lambda_1=\lambda_2=\lambda$ and $\xi_1=\xi_2=\xi$ in the equations of state above. With elimination of the variable $\tilde{D}$ in either Eq. (4) or (5), the function denoting the nominal stress of the membrane is illustrated in Eq. (7).

$$\frac{P}{LH}=\frac{\mu^A(T)(\lambda-\lambda^{-5})}{1-\frac{2\lambda^2+\lambda^{-4}-3}{J^A}}+\frac{\mu^B(T)(\lambda\xi^{-2}-\lambda^{-5}\xi^{4})}{1-\frac{2\lambda^2\xi^{-2}+\lambda^{-4}\xi^{4}-3}{J^B}}\quad\tilde{E}^2\varepsilon_0(1.5a\lambda^2+\ b/T+\ c)\lambda^3 \tag{7}$$

Based on the expression of the nominal stress, a function $F(\lambda)$ that characterizes the elasticity of the elastomer can be obtained in Eq. (8). In the absence of a voltage (E=0), the function $F(\lambda)$ corresponds to the nominal stress $s=P/LH$. In the absence of mechanical loads (s=0), the membrane of DE will also contract in thickness and expand in area when subject to a voltage. The deformation induced by electric filed equals that caused by the Maxwell stress, which is equivalent to the equal-biaxial nominal stress $(1.5a\lambda^2+b/T+c)\lambda^3\varepsilon_0\tilde{E}^2$. The two items in Eq. (8) also represent the nominal stresses of the networks, respectively.

$$F(\lambda)=\frac{\mu^{A}(T)(\lambda-\lambda^{-5})}{1-\dfrac{2\lambda^{2}+\lambda^{-4}-3}{J^{A}}}+\frac{\mu^{B}(T)(\lambda\xi^{-2}-\lambda^{-5}\xi^{4})}{1-\dfrac{2\lambda^{2}\xi^{-2}+\lambda^{-4}\xi^{4}-3}{J^{B}}} \tag{8}$$

The dashpot in the nonlinear rheological model is regarded as a Newtonian fluid, so the rate of deformation in the dashpot can be denoted by $\xi^{-1}\mathrm{d}\xi/\mathrm{d}t$, and the relationship between the stretch λ and the inelastic stretch ξ can be described in Eq. (9). The dashpot will dissipate the mechanical energy with a viscoelastic relaxation time $\tau(T)=\eta/\mu^{B}(T)$ [14], which obviously depends on temperature. Refer to the experiment data from Sheng et. al [36], the viscoelastic relaxation time corresponding to four sampling temperatures are illustrated: τ(273K)=87.216 s, τ(293K)=72.377 s, τ(313K)=67.802 s and τ(333K)=65.573 s.

$$\frac{\mathrm{d}\xi}{\mathrm{d}t}=\frac{\mu^{B}(T)}{6\eta}\frac{\lambda^{2}\xi^{-1}-\lambda^{-4}\xi^{5}}{1-(2\lambda^{2}\xi^{-2}+\lambda^{-4}\xi^{4}-3)/J^{B}} \tag{9}$$

2.2. Equations of the plane-parallel capacitor

When the two electrodes are connected to an electric power source through a conducting wire, charges will be activated and transferred from one electrode to another, leading to the electric potential difference between the surfaces of the DE membrane. Along with the deformation induced by the equal-biaxial force, the additional charges can be stored and released through the electric circuit. From an electrical point of view, the DEG can be regarded as a stretchable plane-parallel capacitor. The membrane of DE functions as a dielectric medium between two compliant electrodes plates. The governing equation for this capacitor is given by $Q_p=\Phi C$, where C represents the capacitance of the DEG determined by the configuration of the DE membrane. By definition, the electric displacement is $D=Q_p/(\lambda L)^2$, and the electric field is $E=\Phi/h$. These two variables can be related by $D=\varepsilon_0\varepsilon_r E$. A combination of the relations above is shown in Eq. (10).

$$Q_P=C\Phi=\left[\frac{L^{2}}{H}\varepsilon_0(a\lambda^{6}+\frac{b}{T}\lambda^{4}+c\lambda^{4})\right]\Phi \tag{10}$$

2.3. Equations of the current leakage

As an electrical component, there is no doubt that the generator made of DE will suffer from unavoidable leakage problem, as shown in Fig. 3. The current leaks through the membrane i_{leak} can be modeled by a conductor which is in parallel with a capacitor. The amount of the current which flows through the electrodes i_p is obtained by differentiating the magnitude of the positive and negative charges $\pm Q_p$ that polarize the membrane with respect to time. The total amount of the charges which transported through the conducting wire is Q and can be acquired by Eq. (11).

$$\frac{\mathrm{d}Q}{\mathrm{d}t}=\frac{\mathrm{d}Q_P}{\mathrm{d}t}+i_{leak} \tag{11}$$

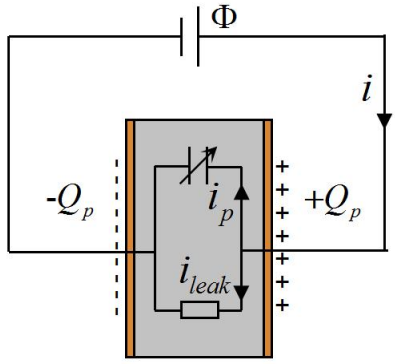

Figure 3. Current leakage model of the DE membrane.

A variable describing the density of the leaked current is defined, $j_{leak}=i_{leak}/(\lambda L)^2$. In addition, the experiment has indicated that the conductivity of the VHB elastomer rises exponentially with the rising electric field, and the following relation has be fitted, $j_{leak}=\sigma_0 \exp(E/E_B)E$ [37], where σ_0 is the conductivity under the low electric fields, and E_B is an empirical constant with the same dimension as the electric field. The variables $\sigma_0=3.32\times10^{-14}$ S/m, $E_B=40$ MV/m are chosen for the following analysis [14][38], and i_{leak} can be obtained from Eq.(12).

$$\frac{i_{leak}}{L^2}=\sigma_0 \exp(\frac{\tilde{E}\lambda^2}{E_B})\tilde{E}\lambda^4 \tag{12}$$

3.Mechanisms of energy conversion and failure modes

Different kinds of processes such as constant voltage, constant charge and constant electric [39]-[41] have been designed as energy conversion cycles. Although each conversion cycle has its own merits and demerits in the suitability and stability, the mechanism of conversion cycles can be summarized: the electrical energy is extracted from a four-stroke cycle by the variability in the capacitance of the DE membrane. To narrow down our research objective, the Carnot-shape cycle [42][43] that consists of two constant voltage processes and two open circuit processes is introduced and employed to study the behaviors of the DEG at different temperatures.

3.1. Basic energy conversion cycle

The Carnot-shape cycle applied to the DEG can be realized via a three-way switch [43][44]. A switch can connect the generator to the input battery that provides the charges at a low voltage, or connect it to the output battery that stores the charges at a high voltage, or keep it in an open circuit. The mechanism of an ideal four-stroke cycle is demonstrated in Fig. 4, where a line describes a process and a contour is a cycle. In the process A→B, as illustrated in Fig. 4(b), the amount of the charges on the electrodes supplied by the low-voltage battery increases from Q_{low} to Q_{high} with the continuous stretch of the membrane from λ_A to λ_B as depicted in Fig. 4(a) (the capacitance improves). In the process B→C, with constant charge (open circuit), the voltage between the electrodes increases when the stretch is partly released from λ_B to λ_C (the capacitance decreases). The release degree is measured by the expression: $\Phi_{low}C(\lambda_B)=\Phi_{high}C(\lambda_C)$. In the process C→D, the charges on the electrodes are pumped to the high-voltage battery due to the further release of the stretch from λ_C to λ_D (the amount of the charges that the DEG can store declines with a smaller capacitance). In the last process, with charges maintained again (open circuit), the voltage between the electrodes decreases when the membrane is stretched from λ_D to the initial stretch λ_A (the capacitance increases) and the

following relation should be satisfied: $\Phi_{low}C(\lambda_A)=\Phi_{high}C(\lambda_D)$. After each cycle, external forces pump a certain amount of charges from the low-voltage battery to the high-voltage one.

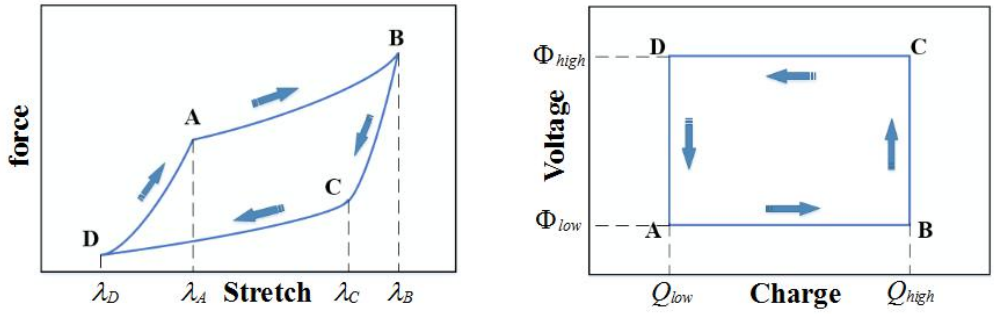

(a) force-stretch diagram (b) voltage-charge diagram

Figure 4. The mechanism of an ideal four-stroke cycle.

In the following analysis, the DEG will be operated in the conversion cycle with four courses: starting with the initial stretch λ_0 at state A, the DEG is subject to a low-voltage battery and an equal-biaxial force stretches the membrane at the same time. The first process ends at state B, in which the maximum stretch achieves λ_{max}. In the process B→C, the low-voltage battery disconnects the membrane and the force is partly released to make the membrane thicker. In the process C→D, a high-voltage battery is applied to the membrane and the force is further released. The minimum stretch λ_{min} is attained at state D. In the last process, the equal-biaxial force stretches the membrane to the initial state in the open circuit condition. The complete energy conversion cycle is sketched in Fig. 5, where the initial state of the DEG is depicted by the color image, and the dotted line indicates the final state.

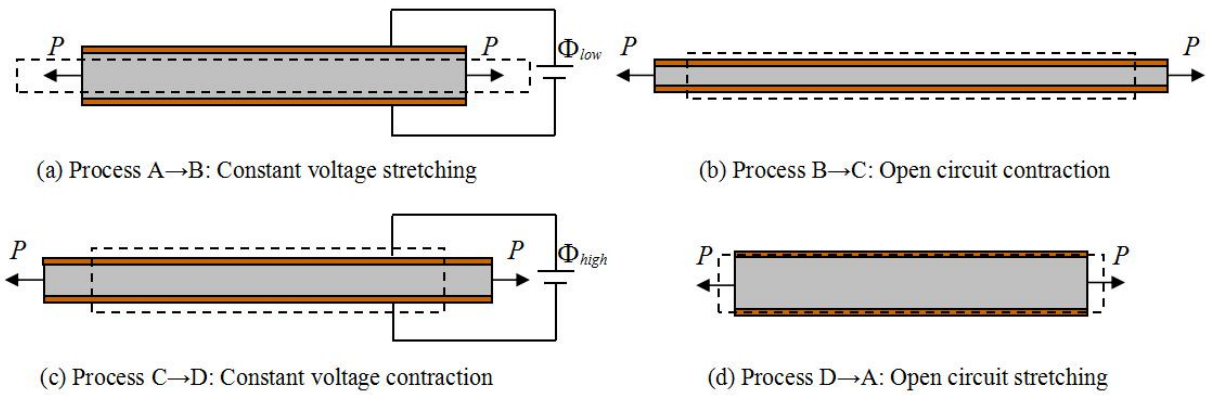

Figure 5. The DEG operates in different processes of the conversion cycle.

The previous study has proved theoretically that the pre-stretch can produce a larger nominal electric field and improve the stability of the elastomer [45]. Thus, the DEG is pre-stretched before activation. Because of viscoelasticity, the mechanical behavior of the DE membrane is affected by the viscoelastic relaxation time. Considering that the relaxation time reaches its maximum 87.216 s at 273 K, so the period of the cycle should be set above this value to give the membrane enough time to fully relax. Here, the period is set as t_{cycle}=90 s. By determining the initial and maximum stretches (λ_0=4 and λ_{max}=6), the stretch at state C (λ_C=4.8), and the low-level voltage Φ_{low}=1.8 kV, the minimum stretch and the high-level voltage are calculated by expressions $\Phi_{low}C(\lambda_{max})=\Phi_{high}C(\lambda_C)$ and $\Phi_{low}C(\lambda_0)=\Phi_{high}C(\lambda_{min})$. However, the capacitance

of the DEG will be altered by temperature, resulting in various results, as can be seen in Tab. 1. For simplicity, the average values are employed and the periods of different courses can be obtained at a constant stretch rate $|d\lambda/dt|=2\times(\lambda_{max}-\lambda_{min})/t_{cycle}$ (t_{AB}=33 s, t_{BC}=20 s, t_{CD}=25 s and t_{DA}=12 s). The stretch applied to the DEG is demonstrated in Fig. 6a, and the nominal electric field solved from Eq. (10) is fitted under different temperature situations and illustrated in Fig. 6b (the curve is assumed to be continuous and independent of temperature).

Table 1. The minimum stretch and high-level voltage calculated at different temperatures.

Temperature	273 K	293 K	313 K	333 K
λ_{min}	3.2954	3.3002	3.3048	3.3091
Φ_{high} (kV)	3.6918	3.6645	3.6389	3.6149

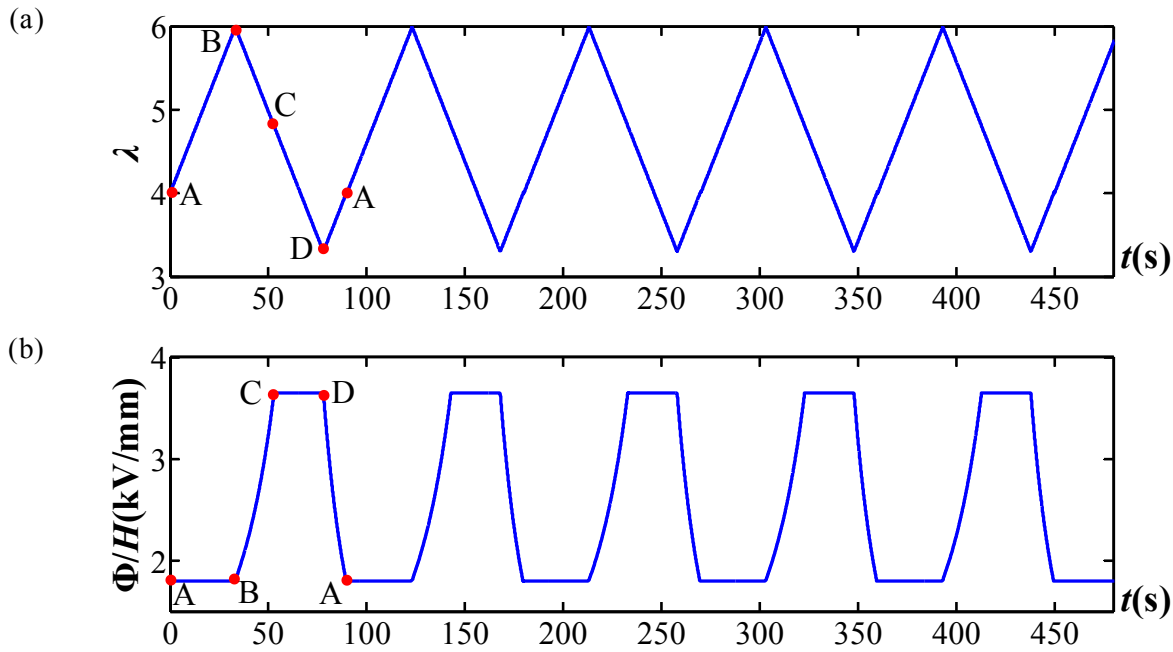

Figure 6. Cyclic loadings for the conversion. (a) The stretch; (b) The nominal electric field;

3.2. Mechanisms of failure modes and verification

As mentioned before, the behavior of the DE membrane is badly restricted by failure modes. Therefore, the cyclic loadings applied in Fig. 6 must locate in the allowable area to ensure the normal function of the DEG [43][44]. In this section, the mechanisms of the common failures are described and the feasibility of the cyclic loadings applied is validated.

3.2.1. Material rupture

The deformation of the DE membrane is finite because of the extension limits of the polymer. When polymer chains are seriously pulled, the chains approach the limit of configuration and the rupture may cause the failure of the generator. The critical stretch of the DEG may also be restricted by the stretch limit of the electrodes. However, more compliant electrodes are used in this work, letting the critical stretch of the generator be the stretch limit of DE. The critical condition for rupture is $\lambda=\lambda_R$, and the previous research has suggested that the critical stretch of VHB 4910 under equal-biaxial stretch is λ_R=6 [46].

3.2.2. Loss of tension

It is vital to maintain the membrane of DE in tension, as wrinkles can be caused easily by any compressive stress in plane, which may affect the normal operation of the DEG. The critical condition for LT is s=0 (P=0), and can be figured out by vanishing the nominal stress in Eq. (7), as illustrated in Eq. (13). Substitute the applied time-dependent stretch into Eq. (13), the boundaries of LT corresponding to different sampling temperatures can be plotted in Fig. 7.

$$\tilde{E}_{LT}^2 = \frac{\dfrac{\mu^A(T)(\lambda-\lambda^{-5})}{1-\dfrac{2\lambda^2+\lambda^{-4}-3}{J^A}} + \dfrac{\mu^B(T)(\lambda\xi^{-2}-\lambda^{-5}\xi^4)}{1-\dfrac{2\lambda^2\xi^{-2}+\lambda^{-4}\xi^4-3}{J^B}}}{\varepsilon_0(1.5a\lambda^2+\dfrac{b}{T}+c)\lambda^3} \tag{13}$$

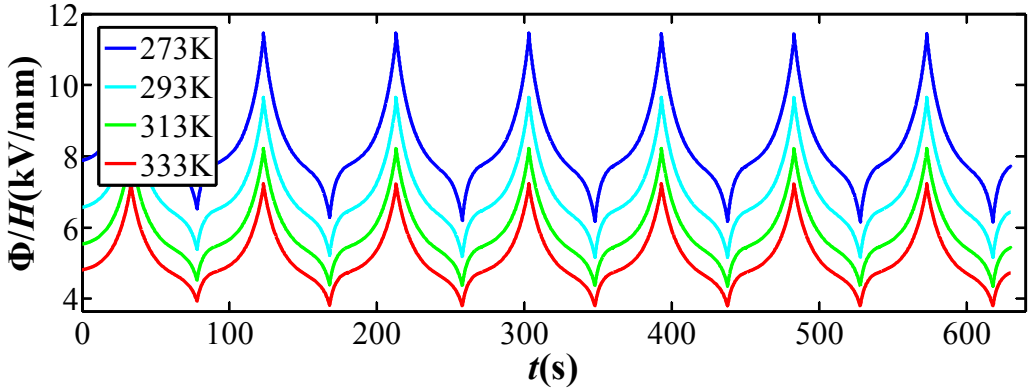

Figure 7. The critical condition for LT at different temperatures.

It is found that the boundary of LT will decline with a higher temperature and gradually reach a steady state after several cycles due to viscoelasticity. In this simulation, the lowest critical value for this failure mode is 3.79×10^6 V/m at T=333K, which is still larger than the highest nominal electric field applied. As a result, no failure of LT will take place.

3.2.3. Electrical breakdown

When the membrane is connected to a voltage source, electrical breakdown may happen with the increasing electric field, making the device fail. The electrical breakdown field is always assumed as constant in the previous studies [42][43], but the latter experiments on the VHB elastomer have indicated that the critical value of electrical breakdown E_{EB} depends on the stretch of DE [47][48], and the experimental data can be fitted in Eq. (14).

$$\tilde{E}_{EB} = E_{EB}(\lambda)\lambda^{-2} = E_{EB}(1)\lambda^{R-2} \tag{14}$$

where $E_{EB}(1)$ is the electrical breakdown field of the membrane of DE in the reference state, and the exponent coefficient R represents the sensitivity of the electrical breakdown field toward the stretch. Parameters for the VHB elastomer with the thickness H=1.0mm are fitted as $E_{EB}(1)$=30.6 MV/m and R=1.13 [20]. Substitute the time-dependent stretch into Eq. (14), it can be easily observed that the smallest critical value for EB 6.44×10^6 V/m is larger than the maximum of the applied nominal electric field, leading to no EB during the harvesting.

3.2.4. Electromechanical instability

Exposure to a voltage, the membrane of DE will compress its thickness, resulting in a higher true electric field. The positive feedback between the true electric field and the thickness may make the membrane thin down sharply, leading to EMI. The boundary of this failure can be defined as: when the mechanical forces are fixed, the voltage becomes a function of stretch. The peak of $\Phi(\lambda)$ corresponds to the critical condition for EMI. Differentiate Eq. (7) with respect to stretch, and the boundaries of EMI can be derived as:

$$\tilde{E}_{EMI}^2 = \frac{\left(\begin{array}{l} \dfrac{\mu^B(\lambda\xi^{-2}-\lambda^{-5}\xi^4)(4\lambda\xi^{-2}-4\lambda^{-5}\xi^4)}{(1-\dfrac{2\lambda^2\xi^{-2}+\lambda^{-4}\xi^4-3}{J^B})^2 J^B} + \dfrac{\mu^A(\lambda-\lambda^{-5})(4\lambda-4\lambda^{-5})}{(1-\dfrac{2\lambda^2+\lambda^{-4}-3}{J^A})^2 J^A} \\ + \dfrac{\mu^B(\xi^{-2}+5\lambda^{-6}\xi^4)}{(1-\dfrac{2\lambda^2\xi^{-2}+\lambda^{-4}\xi^4-3}{J^B})} + \dfrac{\mu^A(1+5\lambda^{-6})}{(1-\dfrac{2\lambda^2+\lambda^{-4}-3}{J^A})} \end{array} \right)}{(7.5a\lambda^4 + \frac{3b}{T}\lambda^2 + 3c\lambda^2)\varepsilon_0} \tag{15}$$

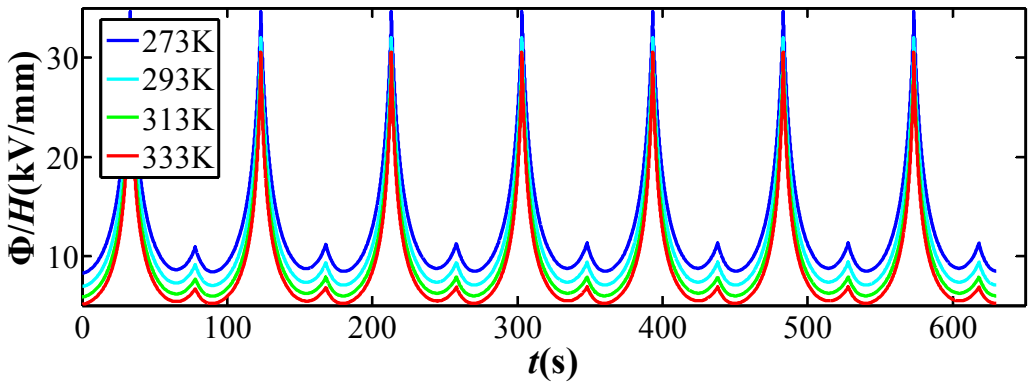

Figure 8. The critical condition for EMI at different temperatures.

Similar to the failure of LT, the boundary of EMI also depends on temperature and a higher temperature lowers the boundary of EMI. According to the numerical results, the minimum critical value for EMI is 5.12×10^6 V/m, which is larger than the highest nominal electric field applied. In summary, for the generator made of VHB 4910, the cyclic loadings applied will not lead to any failures within the temperature range 273K~333K.

4. Temperature effects on the performance of the DEG

Due to obvious viscoelastic relaxation, polymer chains in the membrane of DE will not attain stable configurations instantly. Therefore, it will take the DEG some time to possess steady mechanical parameters such as inelastic stretch and nominal stress. According to Eq. (9), the inelastic stretch can be obtained once the time-dependent stretch is determined. The inelastic stretches at different sampling temperatures are plotted in Fig. 9. It is observed that a higher temperature gives rise to a larger inelastic stretch, and the inelastic stretch will reach the peak value behind stage B in which the peak stretch achieves in every single cycle. Furthermore, the largest inelastic stretch will never exceed λ_{max}, and the curves will attain steady-state after the first five cycles in this study.

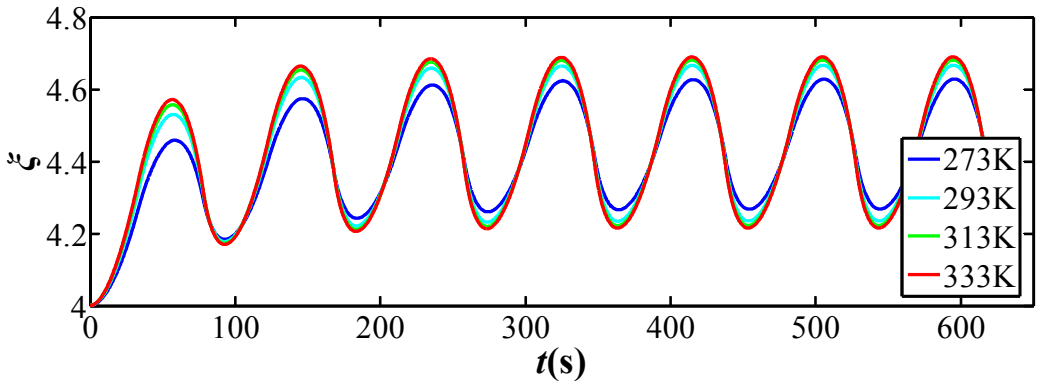

Figure 9. The inelastic stretch as a function of time at different temperatures.

Substitute the time-dependent stretch and inelastic stretch into Eq. (7), the nominal stress as a function of time can be depicted at different temperatures in Fig. 10. The curves show that the membrane of DE necessitates a larger equal-biaxial force at a lower temperature to satisfy the required operating condition. This phenomenon can be explained by the smaller modulus of DE induced by the higher temperature. Similarly, the nominal stress will attain steady-state after the first five cycles.

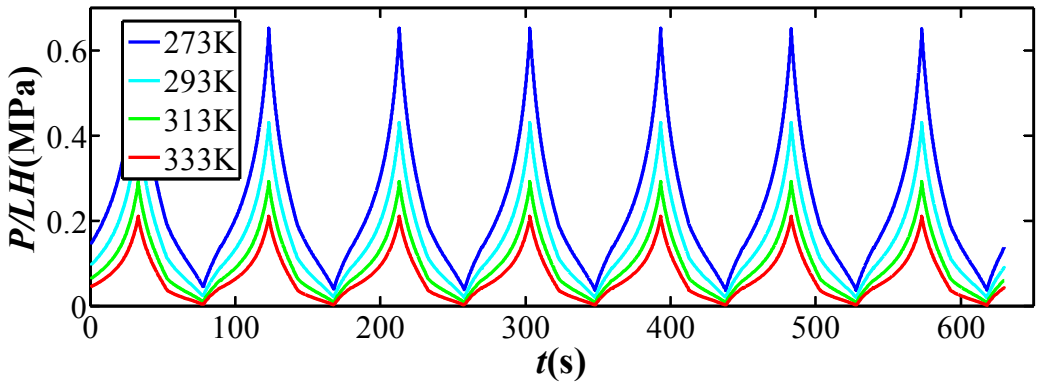

Figure 10. The nominal stress as a function of time at different temperatures.

The amount of the charges on the electrodes $\pm Q_p$ can be calculated from Eq. (10) and the temperature will affect the charges via the permittivity of DE, the factor b/T. The amounts of the charges on the electrodes and the leaked charges at different temperatures are illustrated in Fig. 11. It can be found from the curves that a higher temperature corresponds to a lower level of Q_p due to the negative effect of the temperature on the permittivity, and the amounts of the charges in process B→C and D→A are almost constant for the open circuit conditions. The amount of the leaked charges will increase after every single cycle due to the periodicity of the applied loads. The total amount of the charges through the conducting wire is obtained by the addition of Q_p and Q_{leak}, and will exhibit an increasing tendency as well.

Differentiate the charge-related parameters in Fig. 11 with respect to time, the magnitudes of currents can be solved with temperature variation. Similar to the tendencies of the charges, a higher temperature will make the magnitude of the current through the electrodes decline.

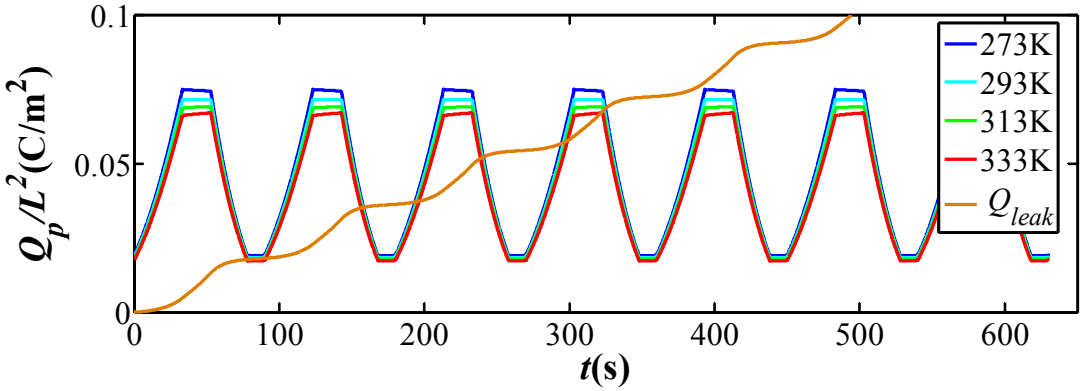

Figure 11. The amount of the charges on the electrodes as a function of time at different temperatures as well as the leaked charges.

For an ideal DEG, the energy input includes the mechanical work done by the equal-biaxial force and the electrical energy provided by the low-voltage battery, and the energy output is measured by the electrical energy pumped to the high-voltage battery. However, during the conversion, some parts of the energy will be lost, including the mechanical energy dissipated by the inelastic stretch and the electrical energy lost by the leaked current. The mathematical expressions of different kinds of energies are described as follows:

The mechanical work done per cycle depends on the stretch of the membrane λ and the magnitude of the equal-biaxial force P, which will attain steady-state after several cycles, as shown in Fig. 10. The total mechanical energy in a single cycle can be calculated by $2\int P\mathrm{d}(\lambda L)$. Since no specific dimensions of the original configuration is defined in this study, it is of great convenience to adopt the energy density to characterize the amplitude of energy. Thus, the mechanical energy density can be presented in Eq. (16).

$$w_{mech}=2\int (P/LH)\,\mathrm{d}\,\lambda \tag{16}$$

The membrane of DE will dissipate the mechanical energy partially through the work done by the dashpot during the deformation. As mentioned before, the stress acting on the dashpot equals the stress in spring B, and the nominal stress of the dashpot is presented by $s^B=\sigma^B/\xi$. Similarly, the energy density of viscous loss w_{visc} is given in Eq. (17). Moreover, the electrical energy dissipated by the current leakage which relies on the magnitude of voltage Φ and the amount of charges that leak through the electrodes Q_{leak} is described in Eq. (18).

$$w_{visc}=2\int s^B\,\mathrm{d}\,\xi \tag{17}$$

$$w_{leak}=\int (\Phi/H)\,\mathrm{d}(Q_{leak}/L^2) \tag{18}$$

Based on the condition of energy flow, the mechanical work done by the equal-biaxial force makes up the absolute input part, the energy dissipated by the inelastic stretch and the leaked current constitutes the loss part, and the difference between the electrical energy pumped to the high-voltage battery and the energy absorbed from the low-voltage battery stands for the absolute output part.

The mechano-electrical conversion efficiency described by α can be obtained from Eq. (19). It is obvious that the efficiency of the DEG operates at α=1 without any losses. If the amount of the energy lost is more than the mechanical energy, the generator will operate at a negative efficiency with no energy generated.

$$\alpha=1-(w_{visc}+w_{leak})/w_{mech} \tag{19}$$

Meanwhile, the electrical energy that contains the electrical energy generated and the energy lost by the leaked current is also figured out to examine the correctness of the energies above. This electrical energy can be calculated from Eq. (20).

$$w_{pele}=-\int(\Phi/H)\,\mathrm{d}(Q_p/L^2) \tag{20}$$

The relevant variables are taken from the seventh cycle (steady-state) in the response curves in Figs. 9-11 to calculate the integrals above. Specifically, the mechanical energy density is integrated over the cycle on the force (P/LH)-length (λ) diagram, as shown in Fig. 12a. The density of the viscous loss is integrated over the cycle on the force (s^B)-length (ξ) diagram, as shown in Fig. 12b. The density of the electrical energy containing the electrical loss and the generated part is integrated over the cycle on the voltage (Φ/H)-charge (Q_p/L^2) diagram, as shown in Fig. 12c. The density of the electrical loss is integrated over any single cycle of the voltage (Φ/H)-charge (Q_{leak}/L^2) diagram, as shown in Fig. 12d.

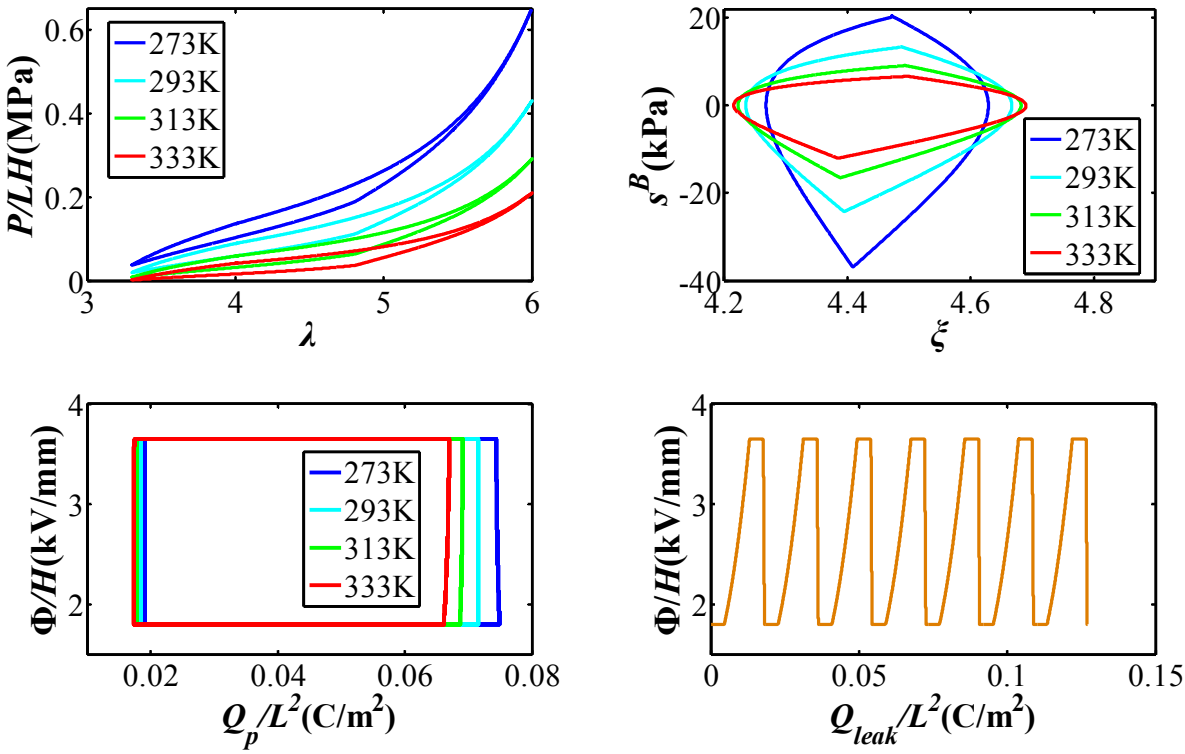

Figure 12. The curves characterize the energies of different kinds. (a) The mechanical energy produced by the force; (b) The energy dissipated by viscoelasticity; (c) The electrical energy involving the electrical loss and the generated part ; (d) The energy loss due to current leakage;

The values of these energy densities at different sampling temperatures are outlined in the following table. The second column of Tab. 2 indicates that the mechanical energy decreases with a higher temperature, and the temperature tends to have less influence on the mechanical energy (the difference of w_{mech} is 9800 J/m^3 from 273 K to 293 K and 7000 J/m^3 from 313 K to 333 K). The third column also shows that the DEG dissipates less mechanical energy at a higher temperature. Due to the direct control on the stretch in this study, the electrical energy lost by current leakage is independent of temperature. The conversion efficiency is listed in the fifth column and it is found that a higher conversion efficiency can be realized if the DEG is operated at a low temperature. The reason is that the reduction in temperature gives rise to relatively more mechanical energy than the viscous loss. However, the temperature effect on the efficiency will get smaller when the temperature keeps rising. The electrical energy which has the same trend as the mechanical energy is also listed in the last column. Furthermore, it is observed that the mechanical energy w_{mech} almost equals the sum of the viscous loss w_{visc} and the electrical energy w_{pele} involving the electrical loss w_{leak} and the absolute output part, satisfying the conservation of energy.

Table 2. Energy densities and conversion efficiency at different temperatures.

T (K)	w_{mech} (J/m^3)	w_{visc} (J/m^3)	w_{leak} (J/m^3)	α	w_{pele} (J/m^3)
273	1.287e+05	2.598e+04	4.842e+04	42.19%	1.027e+05
293	1.189e+05	2.052e+04	4.842e+04	42.01%	9.835e+04
313	1.095e+05	1.521e+04	4.842e+04	41.89%	9.427e+04
333	1.025e+05	1.124e+04	4.842e+04	41.78%	9.124e+04

6. Conclusions

In this study, with combination of the temperature-dependent permittivity and shear modulus and major dissipation processes including viscoelasticity and current leakage, an integrated model focusing on the influences of temperature on the performance of DEGs is established. On the basis of a specific energy conversion cycle, the performance parameters including the energy density and conversion efficiency can be all figured out at various temperatures. It is noticed that the DEG operates more efficiently at a lower temperature owing to the relatively more enhancement in the input mechanical energy than the viscous loss. In the meantime, the failure modes are considered at different temperatures to ensure the normal operation of the device. It is observed that the generator is more likely to suffer from LT and EMI at a higher temperature. The simulation in this study may offer great help and guideline in the design and optimization of energy harvesting with different temperature conditions, which can contribute to a more efficient dissipative DEG.

Acknowledgements

The authors wish to thank the support of National Natural Science Foundation of China (Grant No.61232014) and Project funded by China Postdoctoral Science Foundation. The authors also wish to thank Research Project of State Key Laboratory of Structural Analysis for Industrial Equipment (Grant No.GZ1403), the Science Fund of State Key Laboratory of Advanced Design and Manufacturing for Vehicle Body (Grant No.51375001), and Research Project of State Key Laboratory of Mechanical Systems and Vibration MSV201711.

References

[1]. O'Halloran, A., O'Malley, F. and McHugh, P. (2008) A review on dielectric elastomer actuators, technology, applications, and challenges. *Journal of Applied Physics* **104**, 071101.

[2]. Suo, Z. G. (2010) Theory of dielectric elastomers. *Acta Mechanics Solids Sinica* **23**, 549-578.

[3]. Kornbluh, R. D., Pelrine, R., Prahlad, H., Wong-Foy, A., Mccoy, B. and Kim, S., et al. (2011) From boots to buoys: promises and challenges of dielectric elastomer energy harvesting. *Proceedings of SPIE* **7976**, 67-93.

[4]. Pelrine, R., Kornbluh, R., Pei, Q. and Joseph, J. (2000) High-speed electrically actuated elastomers with strain greater than 100%. *Science* **287**, 836-839.

[5]. Brochu, P. and Pei, Q. (2010) Advances in dielectric elastomers for actuators and artificial muscles. *Macromolecular Rapid Communications* **31**, 10-36.

[6]. Tsuchitani, S., Sunahara, T. and Miki, H. (2015) Dielectric elastomer actuators using Slide-Ring Material® with increased permittivity. *Smart Materials & Structures* **24**, 065030.

[7]. Giousouf, M. and Kovacs, G. (2013) Dielectric elastomer actuators used for pneumatic valve technology. *Smart Materials & Structures* **22**, 104010.

[8]. Adrian Koh, S. J., Keplinger, C., Li, T. F. and Bauer, S. (2011) Dielectric Elastomer Generators: How Much Energy Can Be Converted? *IEEE/ASME Transactions On* **16**, 33-41.

[9]. Lv, X. F., Liu, L. W., Liu, Y. J. and Leng, J. S. (2015) Dielectric elastomer energy harvesting: maximal converted energy, viscoelastic dissipation and a wave power generator. *Smart Materials & Structures* **24**, 115036.

[10]. Kornbluh, R. D. and Pei, Q. (2001). Dielectric elastomers: generator mode fundamentals and applications. *Proceedings of SPIE* **4329**, 148-156.

[11]. Rome, L. C., Flynn, L., Goldman, E. M. and Yoo, T. D. (2005) Generating electricity while walking with loads. *Science* **309**, 1725-1728.

[12]. Jean-mistral, C. (2008). Dielectric polymer: scavenging energy from human motion. *Proceedings of SPIE* **6927**, 692716-692716-10.

[13]. Chiba, S., Waki, M., Kornbluh, R. and Pelrine, R. (2009) Innovative wave power generation system using electroactive polymer artificial muscles. *Oceans IEEE*, 1-3.

[14]. Chiang Foo, C., Cai, S., Koh, S. J. A. and Bauer, S. (2012) Model of dissipative dielectric elastomers. *Journal of Applied Physics* **111**, 836-382.

[15]. Liu, L. W., Zhang, Z., Liu, Y. J. and Leng, J. S. (2014) Failure modeling of folded dielectric elastomer actuator. *Science China Physics, Mechanics & Astronomy* **57**, 263-272.

[16]. Zhao, X. H. and Suo, Z. G. (2007) Method to analyze electromechanical stability of dielectric elastomers. *Applied Physics Letter* **91**, 061921.

[17]. Zhou, J., Jiang, L. and Khayat, R. E. (2014) Electromechanical response and failure modes of a dielectric elastomer tube actuator with boundary constraints. *Smart Materials & Structures* **23**, 045028.

[18]. Sheng, J. J., Chen, H. L. and Li, B. (2011) Effect of temperature on the stability of dielectric elastomers. *Journal of Physics D Applied Physics* **44**, 365406.

[19]. Liu, L. W., Liu, Y. J., Yu, K. and Leng, J. S. (2014) Thermoelectromechanical stability of dielectric elastomers undergoing temperature variation. *Mechanics of Materials* **72**, 33-45.

[20]. Plante, J. S. and Dubowsky, S. (2006). Large-scale failure modes of dielectric elastomer actuators. *International Journal of Solids & Structures* **43**, 7727-7751.

[21]. Keplinger, C., Li, T. F., Baumgartner, R., Suo, Z. G. and Bauer, S. (2012) Harnessing snap-through instability in soft dielectrics to achieve giant voltage-triggered deformation. *Soft Matter* **8**, 285-288.

[22]. Leng, J. S., Liu, L. W., Liu, Y. J., Yu, K. and Sun, S. H. (2009) Electromechanical stability of dielectric elastomer. *Applied Physics Letters* **94**, 211901.

[23]. Zhao, X. H., Adrian Koh, S. J. and Suo, Z. G. (2011) Nonequilibrium thermodynamics of dielectric elastomers. *International journal of Applied Mechanics* **3**, 203-217.

[24]. Li, B., Zhang, J., Liu, L. and Chen, H. (2014). Modeling of dielectric elastomer as electromechanical resonator. *Journal of Applied Physics* **116**, 124509-124509-9.

[25]. Qiang, J. H., Chen, H. L. and Li, B. (2012) Experimental study on the dielectric properties of polyacrylate dielectric elastomer. *Smart Materials & Structures* **21**, 025006.

[26]. Jean-Mistral, C., Sylvestre, A., Basrour, S. and Chaillout, J. J. (2010) Dielectric properties of polyacrylate thick films used in sensors and actuators. *Smart Materials & Structures* **19**, 075019.

[27]. Zhao, X. H., Hong, W. and Suo, Z. G. (2007) Electromechanical coexistent states and hysteresis in dielectric elastomers. *Physics Review B* **76**, 1283.

[28]. Zhang, J. S., Tang, L. L., Li, B., Wang, Y. J. and Chen, H. L. (2015) Modeling of the dynamic characteristic of viscoelastic dielectric elastomer actuators subject to different conditions of mechanical load. *Journal of Applied Physics* **117**, 084902.

[29]. Wang, H. M., Lei, M., and Cai, S. Q. (2013) Viscoelastic deformation of a dielectric elastomer membrane subject to electromechanical loads. *Journal of Applied Physics* **113**, 213508-213508-7.
[30]. Zhang, J. S., Chen, H. L., Tang, L. L., Li, B., Sheng, J. J. and Liu, L. (2015) Modeling of spring roll actuators based on viscoelastic dielectric Elastomers. *Applied Physics A*. **119**, 825-835.
[31]. Zhou, J. Y., Jiang, L. Y. and Khayat, R. E. (2014) Viscoelastic effects on frequency tuning of a dielectric elastomer membrane resonator. *Journal of Applied Physics* **115**, 124106-124106-11.
[32]. Li, B., Chen, H. L., Qiang, J. H. and Zhou, J. X. (2012) A model for conditional polarization of the actuation enhancement of a dielectric elastomer. *Soft Matter* **8**, 311-317.
[33]. Gent, A. N. (1996) A new constitutive relation for rubber. *Rubber Chemistry and Technology* **69**, 59-61.
[34]. Michel, S., Zhang, X. Q., Wissler, M., Löwe, C. and Kovacs, G. (2010) A comparison between silicone and acrylic elastomers as dielectric materials in electroactive polymer actuators. *Polymer international* **59**, 391-399.
[35]. Vu-Cong, T., Jean-Mistral, C. and Sylvestre, A. (2013) New operating limits for applications with electroactive elastomer: effect of the drift of the dielectric permittivity and the electrical breakdown. *SPIE - the international Society for Optical Engineering* **30**, 793-806.
[36]. Sheng, J. J., Chen, H. L., Liu, L., Zhang, J. S., Wang, Y. Q., and Jia, S. H. (2013) Dynamic electromechanical performance of viscoelastic dielectric elastomers. *Journal of Applied Physics* **114**, 134101-134101-8.
[37]. Bergamini, A. (2011) Dielectric and insulating properties of an acrylic DEA material at high near-DC electric fields. *Proceedings of SPIE* **7976**, 79763B-79763B-6.
[38]. Gisby, T. A., Xie, S. Q., Calius, E. P. and Anderson, I. A. (2010) Leakage current as a predictor of failure in dielectric elastomer actuators. *Proceedings of SPIE* **7642**, 764213-764213-11.
[39]. Graf, C. and Maas, J. (2011) Evaluation and optimization of energy harvesting cycles using dielectric elastomers. *Electroactive Polymer Actuators & Devices* **7976**, 541-558.
[40]. Graf, C., Maas, J. and Schapeler, D. (2010) Energy harvesting cycles based on electro active polymers. *Proceedings of SPIE* **7642**, 579-595.
[41]. Graf, C., Eitzen, L. and Maas, J. (2011). Multilevel high voltage converter driving dielectric elastomer generators. *European Conference on Power Electronics and Applications IEEE Xplore*, 1-10.
[42]. Chiang Foo, C., Adrian Koh, S. J., Keplinger, C. and Kaltseis, R. (2012). Performance of dissipative dielectric elastomer generators. *Journal of Applied Physics* **111**, 836-839.
[43]. Adrian Koh, S. J., Zhao, X. H. and Suo, Z. G. (2009) Maximal energy that can be converted by a dielectric elastomer generator. *Applied Physics Letter* **94**, 262902-262902-3.
[44]. Bortot, E., Gei, M. and Debotton, G. (2015) Optimal energy harvesting cycles for load-driven dielectric elastomer generators under equibiaxial deformation. *Meccanica* **50**, 2751-2766.
[45]. Wissler, M. and Mazza, E. (2005) Modeling of a pre-strained circular actuator made of dielectric elastomers, *Sensors and Actuators A: Physical* **120**, 184-192.
[46]. Sommer-larsen, P., and Kofod, G. (2002). Performance of dielectric elastomer actuators and materials. *Proceedings of SPIE* 158-166.
[47]. Kofod, G., Sommer-larsen, P., Kornbluh, R. D. and Pelrine, R. (2003). Actuation response of polyacrylate dielectric elastomers. *Journal of Intelligent Material Systems & Structures* **14**, 787-793.
[48]. Tröls, A., Kogler, A., Baumgartner, R., Kaltseis, R., Keplinger, C. and Schwödiauer, R., et al. (2013). Stretch dependence of the electrical breakdown strength and dielectric constant of dielectric elastomers. *Smart Materials & Structures* **22**, 104012.